Contract No.:

This manuscript has been authored by Savannah River Nuclear Solutions (SRNS), LLC under Contract No. DE-AC09-08SR22470 with the U.S. Department of Energy (DOE) Office of Environmental Management (EM).

SRNL-STI-2021-00107

MICROSTRUCTURAL EVOLUTION DURING A SOLID STATE TUBE PINCH WELD OF TYPE 304L STAINLESS STEEL

Paul S. Korinko
Savannah River National Laboratory
Aiken, South Carolina, USA

February 2021

Keywords: Pinch Welding, Stainless Steel,

For publication in Journal of Pressure Vessel Technology

MICROSTRUCTURAL EVOLUTION DURING A SOLID STATE TUBE PINCH WELD OF TYPE 304L STAINLESS STEEL

Korinko, Paul S.[1]
Savannah River National Laboratory
SRNL
Building 773-41A, Rm 240
Aiken, SC 29808
Paul.korinko@srnl.doe.gov
ASME Member PVP 000004175345

ABSTRACT

Microstructure development is examined for a specialized spot weld that is used as a solid-state closure process for austenitic stainless steel tubing, referred to as pinch welding. In order to elucidate the microstructural evolution of the weld, a series of test welds were made at nominal conditions using tubing and production like components. These pinch welds normally terminate after twelve cycles of a 60 Hz AC weld process. In this study, production tubes were welded from one to twelve cycles and the microstructure and weld variables after each individual weld cycle number were characterized using radiography and optical metallography. Two electrochemical etchants were used to highlight different microstructural features. The study revealed that: (1) this type pinch weld is largely complete after about six cycles of 60 Hz AC current, half the weld time utilized; (2) the resistance, deformation, and closure length approach "steady state" conditions after six cycles; and (3) both oxalic and nitric acid electrolytic etchants are useful for highlighting specific microstructural attributes of type 304L stainless steel. Finally, two distinct microstructural regions can be identified for these welds: the edge of the weld which is driven by concentrated deformation, recrystallization, and grain growth and the center region which is more typical of forge welding and micro-asperity breakdown followed by diffusion and grain-growth.

[1] Corresponding author information can be added as a footnote.

INTRODUCTION

Pinch welding is a unique application of a resistance spot weld for closure of gas filled cylinder tubes. This welding method is also known as tube closure welding and particularly suited for use in (potentially hazardous) gas storage cylinder (e.g. hydrogen), where particulate generation is to be avoided, and the application does not allow for typical tubulation through standard pressure fittings. Pinch welding uses bull nose electrodes with either 2.4 mm (3/32 inch) or 4.8mm (3/16 inch) radius electrodes. In one type of pinch welding, the tubes are confined from lateral spread during the weld with a confining die; i.e., it is a confined pinch weld (CPW). The final weld thickness is also limited by the thickness of the confining dies, 1.27 mm (0.050 inch). The confined weld is used for critical applications and where mating components have a matching 3.2 mm (0.125 inch) hole as a receptor. Unconfined welds allow the tube to spread to diameters between 4.06 mm (0.16 inch) and 6.1 mm (0.24 inch) with thicknesses between 0.787 mm (0.031 inch) and 1.24 mm (0.049 inch). Unlike the traditional spot welds, the pinch welds are ideally solid-state welds [1-3]. The rationale for maintaining solid state welds is that the stems are used to seal hydrogen gas containers and solid-state welds reduce the amount of hydrogen that is absorbed in the weld metal. In addition, avoiding melting, reduces the propensity to form weld expulsions and particulates that may have an adverse effect on the component functionality.

A number of studies have been conducted at the Savannah River National Laboratory to better understand fabrication, damage, welding parameters and other influences on

pinch welding. These engineering studies [4-12] show the effects of fill stem manufacturing practices on pinch weld quality. It was shown that machining oils can cause significant defects in the welds when the starting stock (forgings, tubing, bar stock, etc.) is not properly cut and smeared metal occurs which causes multiple interfaces that are not adequately cleaned or removed [4,5,6]. In an attempt to remove internal, loosely adherent particles or oxide films, rotary brushing was attempted. This treatment caused the spread of internal contamination and promoted a lower quality weld than leaving low levels of contaminants [7]. Internal scratches are also of concern, so a detailed study showed that gouges as deep as 38 μm (0.0015") can be welded over without adverse effects. Defects this deep are an order of magnitude greater than any defects found in the actual hardware [8].

The present method of pinch welding utilizes a weld controller essentially as a timer to start and stop the weld after 12 60 Hz cycles (0.2 s) using 100% weld heat and a powerstat to adjust the primary voltage. Research was conducted to evaluate the weld controller's ability to control the weld using constant current where the waveform is chopped to maintain a constant current. These tests revealed that the process is sufficiently robust and the requirements readily achieved that the control mode was not detectable using the metrics selected [9]. The effect of welding atmosphere, i.e., deuterium or air, indicated that there was little influence on the bond line appearance between the two atmospheres [10]. These corporate studies demonstrated that the pinch weld process is highly robust, yet occasionally unacceptable weld attributes are

detected. Thus additional work to elucidate pinch weld quality attributes from the data was conducted. For instance, the weld inputs and outputs were characterized and modeled using a neural network that was able to correctly forecast weld bond line quality after proper training [11], in addition to process modeling [12]. Residual stresses of pinch welds have also been measured [13].

The deformation and recrystallization characteristics of pinch welds have been studied [14]. This study revealed that there is less grain growth across the grains than would be expected based on metallographic analysis. Based on the current description of pinch welding and the evolution of the bond line, one would expect a significant amount of diffusion across the bond interface, the referenced study indicated that grains did not grow across the interface as evidenced by the discontinuity in the crystallography of the grain across the interface.

In general, these studies provided engineering solutions to specific questions related to pinch welds. The evolution of the pinch weld and the microstructural events occurring during the weld were of interest though. Consequently, this study was envisioned and a systematic characterization of the weld microstructure as a function of weld cycles was conducted.

MATERIALS AND METHODS

Pinch welds were made on forged Type 304L stainless steel (SS) stems with the geometry shown in Fig. 1. The stems met all the dimensional and chemistry

requirements to be production components. The welds are made by inserting the stem into a weld fixture and tightening the confining anvils to 9.5 N-m (7 ft-lbs) of torque, a fill stem loaded into the weld fixture is shown in Figure 2. The hole in the front of the fixture is the location for the welding electrode to make mechanical and electrical contact with the stem.

Pinch welds were made using the Savannah River National Laboratory (SRNL) pinch welder shown in Figure 3. This welder contains a prototypic production weld head and with a Heidenhain displacement gauge which is not present on the production welders. The weld head can apply forces up to approximately 7560N (1700 lbs.) and currents up to 5000A and operates on 60 Hz alternating current. The weld heat input is controlled by limiting the input (primary) voltage and monitoring the welding current, i.e., constant voltage mode, using a 480 V powerstat. The energy is calculated within custom LabView control software and is presented with the post weld data metrics, as is the dynamic resistance, current, voltage, and current.

The welds on the fill stems were made using standard fixtures with full restraint (the end of the stem was immovable along its axis) at the fill nubbin and partial restraint at the foot end; a single weld was made in each stem; the same conditions that are used for production products. The confined pinch welds were made using constant voltage control for all number of cycles of 60 Hz AC current between 1 and 14 to observe how the pinch weld microstructure evolves with time/number of weld cycles. In this control

mode, the primary voltage (480V) from the powerstat is reduced to the target voltage (415 V) and the secondary current is directly related to the input voltage. This method of controlling the weld heat has been used for pinch welds for over 60 years. The welds are completed by applying the force to the electrode which crushes the tube, the current is applied, and the faying surfaces interact to form the weld. Since AC current is used, the tube has been observed using high speed video to achieve red heat to no heat color each half 60 Hz cycle.

The electrodes used for pinch welding are wrought copper with brazed tungsten tips and machined to a 4.8 mm (3/16 inch) bull nose. An electrode force of 5560 N (1,250 lbs.) was selected to weld the samples at a target current of 3850 amperes for both the tubing and the stems. The stems were welded at 415 V. To prevent or at least minimize oxidation of the interfaces during welding, nitrogen gas was passed through the stems during processing. This environment has been shown to protect the welds from oxidation and provide a similar welding environment to hydrogen within tubes [9]. The thickness of the welds was measured using a point micrometer, and the closure length was determined using digital radiography. The radiographs were inspected for material extrusion at the end of the welds and expulsion. Metallographic samples were prepared transverse to the tube axis near the center of the weld. The samples were mounted in epoxy, ground, and polished using standard metallographic sample preparation techniques for cross-sectional microscopic examination. The metallographic samples were prepared by grinding from 240 to 600 grit silicon carbide

paper and polished to 1 μm diamond and then electrolytically etching with 10% oxalic acid at a current density of 0.2 mA/cm2 for 15 to 90s. The stems were examined with an optical microscope at magnifications from 50 to 500 times. After initial microscopy, all the stem samples were re-polished and electrolytically etched with 30% nitric acid at 1.2V and reexamined at magnifications to 1000X. The nitric acid etching required multiple iterations of etching and polishing with one μm diamond slurry to reveal a scratch free microstructure. All the tubing samples were examined using optical microscopy in the transverse orientation after electrolytically etching with oxalic acid; these samples were imaged using differential interference contrast.

RESULTS

The starting microstructure for the fill stem is shown in Figure 4 after etching with two different acids. The as-received stems have equiaxed grains, with some annealing twins evident. The stems did not exhibit deformation twins. The stems have a specification requirement of a grain size of ASTM of five or finer and a Rockwell A hardness of 47-58 HRA.

The weld data, the set point and output, for the stems are presented in Table 1 and in Fig. 5. The measured current is less than the target for the first several cycles. This partly results from the controller operation and the calculation of the reported RMS current. For example, the peak current for the first cycle is about 3804 A compared to the target RMS current of 3850 A. The RMS current is calculated by the data acquisition system (DAS) to be 2573 A compared to 2690 A determined by simply dividing the peak

current by the square root of two. Statistical analysis of pinch weld data currents at nominally 3750 A exhibit a standard deviation of 4.4 A.

Dimensional Results

The thickness and closure length results for the stems are listed in Table 2. As expected, the thickness decreases with increasing number of cycles and the closure length increases with increasing cycles. These data are also shown in Figure 6. In a complementary study, it was shown that the thickness at zero cycles depends on the material hardness, but the final weld thickness stabilizes at about 1.19 mm (0.047 inch), regardless of initial hardness. The final thickness is limited by the presence of the Hastelloy X confining dies, and the extent of "ear" formation, material extruded around the confining dies due to deformation of the tube. In the case of fully completed welds, the confining dies act like a positive stop for the stem collapse so this dimension is limited by the equipment geometry.

The X-ray closure measurements indicate no closure occurs for the first several cycles, which is consistent with the metallurgical results discussed below and observations during welding in flowing gas. The radiographic closure lengths were determined from face and side view radiographs, Figure 7.

Metallographic Results

Metallographic samples were prepared and examined for every test weld. Samples were electrolytically etched with oxalic acid and examined, then re-prepared and electrolytically etched with nitric acid and examined. These etchants bring out different features as can be seen in Figure 8 for the stem sample after 3 cycles. The oxalic acid

etched sample indicates that fine grains may be present but does not show them as clearly as the nitric acid etch. Oxalic etching reveals clear evidence of deformation twinning in the bulk away from the weld interface, as well as plastic deformation bands. On the other hand, the nitric acid etch shows numerous fine grains at the interface and in the heavy deformation zone at the tube wall and primary crush zone, also called the "crow's foot", while there is little evidence of either flow lines or deformation twins. The term crow's foot refers to the end of the weld where the tube is initially crushed; this term is used since it often resembles a crow's foot with several dark etch lines or folds. Thus, the use of both etchants provides complementary information to characterize the metallurgical structure of these welds as each display different metallurgical / microstructural attributes.

Various characteristics of the weld microstructure evolution were determined using different magnifications at differing locations across the weld interface. In particular, the extent of recrystallization was clearly revealed from the 500X magnification images of "crow's foot" of the stem welds. Other characteristics, such as the grain size, flow lines, and the presence of recrystallized grains required higher or lower magnifications to reveal the desired details. Some photomicrographs were taken at 1000X in order to resolve the very fine grains present in the samples welded at up to four cycles. The grain size was measured in the crow's foot, (Fig. 8), while in the width of the heat affected zone (HAZ), the area in the center of the weld that exhibits microstructure changes, was

at the weld center (Fig. 9). Near the center recrystallization was initiated at about the fourth cycle, when the faying surfaces contacted and continued until about the 9 cycle.

The weld evolution can be described with cold work crushing the tube and the presence of deformation and twinning in the crow's foot. At the first cycle, the grains in the crow's foot become elongated but the faying surfaces are not in contact. At second cycle, etch pits are visible along the high deformation zone. It is not clear if the etch pits are due to dislocation alignment or the onset of recrystallization. The tube faying surfaces are still not in contact. Recrystallization occurs at the third cycle and the tube collapses and nearly makes contact along the entire surface. At the fourth cycle, the onset of grain growth occurs in the crow's foot and consistent with the X-ray results, there is bonding across the entire faying surface, and some recrystallization. Grain growth continues until about cycle 8 and then there is a stabilization of the grain size. Several welds after a few cycles that exhibit the changes in the microstructure are shown in Figure 8 for the crow's foot and the at the center of the weld in Figure 9.

The grain size and HAZ width were determined from the nitric acid etched samples. It is postulated that these data and attributes could be modeled using common thermal process phenomenology for nucleation and growth, such as the generalized Avrami equation [15]. The grain size and HAZ data for the stem samples are shown graphically in Figure 11. These data show a non-linear response with number of cycles. They also show a delay, perhaps an incubation period, before there are changes in the response.

The grain size and HAZ width dimensions rate decreases after nine cyles. These are likely associated with the total heat input of the weld.

Weld Parameter Results

The primary method of demonstrating acceptable welding in production is to verify that the weld parameters-RMS voltage, electrode force and number of cycles, are within acceptable limits. The limits of each parameter are determined by test welds. One calculated quantity that may provide additional information about weld quality is the so-called “dynamic” resistance. This quantity is calculated by dividing the peak voltage by the peak current during each cycle. A plot of the “dynamic” resistance for the stems as a function of cycles is shown in Figure 12. The dynamic resistance increases from cycle 1 to cycle 2, and then monotonically decreases during subsequent cycles, finally becoming approximately constant at about ten cycles. These results are consistent with a twelve cycle weld that is continuous. Similar to the dynamic resistance, the weld voltage measured across the electrodes peaks at the first cycle and gradually decreases with subsequent cycle. There is a slight shift in the time at which the peak current and peak voltage are detected, but the difference was on the order of one or two tenths of a millisecond. This offset in the time of the voltage and current maxima is an indication of capacitive and inductive components of the system electrical impedance.

The electrode displacement and weld current data are plotted in Figure 13. The deformation during the first cycle is approximately 30% of the total deformation that occurs. A significant amount of thermal softening occurs during this cycle. It is apparent

that more than 70% of the total displacement occurs during the first six weld cycles with the remaining 30% occurring after the seventh cycle. The electrode displacement is also loosely correlated with the closure length increasing during the latter cycles, based on closure data provided in Table 3. It is interesting to note that the electrodes continue to indicate movement after the heat source is shut off. This continued movement may be due to conduction of the heat away from the weld interface and into the surrounding metal which promotes additional deformation of the tube axially to increase the bond length or simply due to thermal contraction of the weld.

DISCUSSION

The weld microstructure evolves differently in the “crow’s foot” (weld edges, Fig. 8) compared to the center of the pinch weld (Fig. 9). The crow’s foot is driven by plastic strain from the shearing and collapse of the tube, recrystallization due to extensive localized deformation and heating, followed by grain growth. The center section of the weld is similar to forge welding with normal forces and interfacial heating. The temperature of the weldment increases as current is passed around and through the collapsed area. The force is applied and then the current, which heats the tube and brings the faying surfaces into intimate contact and promotes oxide breakdown, recrystallization and grain growth.

At the crow’s feet, there is a high degree of plastic flow including extrusion of the side wall surfaces into the bond interface (Fig. 8). This area heats first and also has the highest plastic strain due to the constraint. This complex deformation creates new fresh

surfaces and assists in disrupting and damaging the existing metal surface oxides and contamination. These intimately contacting and freshly cleaned surfaces are able to form a diffusional bond. The extensive and rapid recrystallization initiated in the crow's foot and beyond, promotes microstructural homogeneity across the interface.

In the center of the weld, the confining dies and process geometry limit the extent of deformation in the transverse direction and the way the tube is fixtured in the welder limits the axial expansion to about 0.38 mm (0.015"). Hence, surface disruption in this area occurs primarily on a micro-asperity scale, and the break-up of surface oxides and contamination is less than at the edge areas. The Joule heating may be more intense in this area due to interfacial heating. Fusion welds and expulsion defects are observed near the center of the weld. These defects are often generated at lower forces and high current (i.e., hot welds). Recrystallization will homogenize the microstructure across the bond interface, provided the interfacial grain boundaries are not pinned by inclusions. (Inclusions are quite stable in stainless steels and are not solutionized during pinch welding). It appears that the bonding in the center area of the weld is initially poor and progresses to a diffusional bond as the number of cycles increases. The bond evolves to a situation much like the conditions described in the acceptance criteria, from a distinct bond line with no recrystallization and grain growth to an obscured or completely consumed bond line with extensive recrystallization and grain growth with little or no evidence of a prior interface. However, for solid state bonds with no incipient melting,

like those prepared for this study, the center of the weld is formed with less deformation and is potentially of slightly lower quality than the edges.

CONCLUSIONS

The evolution of microstructure changes with time occurs by two mechanisms for solid state pinch welds. The edges or crow's feet are driven by mechanical and thermal processes while the center is controlled primarily by Joule heating.

Extensive deformation promotes recrystallization between one and three heat cycles. The pinch weld deformation is approximately 80% complete after six cycles. The major recrystallization and grain growth events are completed after eight cycles. The grain size continues to increase but at a much lower rate.

The cycle to cycle resistance as determined by peak V divided by Peak I is reduced through about six cycles at which point it reaches a plateau. This lack of change is consistent with the relative stasis that is observed in the microstructure.

Nitric and oxalic acid etchants are complementary and reveal different features of pinch weld microstructures.

ACKNOWLEDGMENT

The authors would like to acknowledge the contributions and technical input from B. West of Savannah River Tritium Enterprise and the recognize the contributions of the Materials Test Facility (MTF) technicians and Carol Kestin for conducting and

interpreting the metallography, the Materials Technology Section metallographer (Tony Curtis) and assistants for additional metallography and J. Levings for funding the Project NORMAN task as part of the Technology Investment Program. We would also like to recognize the contributions of Daniel Hartman, Vivek Dave, Mark Cola, and Bill King for critical reviews and insightful comments.

FUNDING

This document and the research were prepared and conducted for the U.S. Department of Energy under contract number DE-AC09-08SR22470 with Savannah River Nuclear Solutions.

NOMENCLATURE

A	Ampere
Hz	Hertz
PW	Pinch Weld
SS	Stainless Steel
CPW	Confined Pinch Weld

REFERENCES

[1] Kianersi, Danial, Mostafaei, Amir, Amadeh, Ahmad Ali, “Resistance spot welding joints of AISI 316L austenitic stainless steel sheets: Phase transformations, mechanical properties and microstructure characterizations,” Materials and Design 61 (2014) 251–263
[2] Karcı, Feramuz, Kac¸ Ramazan, Gündüz, Süleyman, “The effect of process parameter on the properties of spot welded cold deformed AISI304 grade austenitic stainless steel,” Journal of Materials Processing Technology 209 (2009) 4011–4019.
[3] Moshayedi, Hessamoddin, & Sattari-Far, Iradj “Numerical and experimental study of nugget size growth in resistance spot welding of austenitic stainless steels,” Journal of Materials Processing Technology 212 (2012) 347– 354.
[4] Korinko, P.S. & Arnold, K.F., Optimization Study for Fill Stem Manufacturing and Pinch Weld Processing, SRNL Report, September 2006
[5] Korinko, P. S., and Maxwell, D N., Fill Stem Manufacturing Changes and Pinch Weld Qualifications, SRNL Report, Feb 21, 2008
[6] Korinko, P. S., and Maxwell, D N., Pinch Weld Testing to Support Change in Manufacturing Oil at the KCP, SRNL Report,, Feb 21, 2008
[7] Korinko, P.S., Effect of Brushing on Pinch Weld Quality, SRNL Report, September 2005. (12-15-05)
[8] Korinko, P.S., Effect of Scratches on Pinch Weld Quality, SRNL Report, September 2005. (11-10-05)
[9] Korinko, P.S. & Howard, S. R., Effect of Constant Current on Pinch Welds, SRNL Report, September 2005.
[10] Korinko, P.S., Effect of Atmosphere on Pinch Weld Quality, SRNL Report, Sept. 2005
[11] Bowers, J.A., and Korinko, P.S., Exploration of Summary Data Sheets of Pinch Weld Experiments and Draft Neural Network Models Forecasting Weld Closure Length, SRNL Report, October 2003.
[12] Hartman, D.A., Korinko, P.S., Tolk, N.R., Malene, S.H., Smith, M.G., Cola, M.J., Dave’, V.R., Miller, J.P., & King, W. H., In-Process Monitoring of Pinch Welding: An Investigation into a Bond Quality Metric, 7th International Conference on Trends in Welding Research, May 16-20, 2005 -- Pine Mountain, Georgia, USA
[13] Korinko, P.S., Pechersky, M.J., Zeha, D.L., McKinney, G.J., Reister, L, Blau, P., Lara-Curzio, E., “Characterization of Confined Pinch Welds in Type 304L Stainless Steel”, 6th International Conference on Trends in Welding Research, 15-19, April 2002, Callaway Gardens Resort, Pine Mountain, Georgia USA", ASM International
[14] Necker, C. T., Marchi, A.N., Smith, M.G., Multi-cycle Pinch Welding of 304L Tubes: Inhomogenieties in Deformation and Recrystallization Textures and Microstructures”, ICOTOM 15, June 1- 6, 2008, Pittsburgh, PA.
[15] Porter, D.A. and Easterling, K.E., Phase Transformations in Metals and Alloys, Van Nostrand Reinhold, UK, 1981.

Figure Captions List

Fig. 1 Schematic of a typical fill stem

Fig. 2 Stem and confining dies used in this study to make confined pinch weld

Fig. 3 Weld head used in this study, a indicates the PW electrode, b the ram that applies the force, and c the weld fixture support

Fig. 4 Initial microstructure of the stem electrolytically etched with a) nitric acid showing the grain size and b) etched with oxalic acid showing other microstructural details

Fig. 5 Plot of weld conditions, data from Table 1

Fig. 6 Dimensional measurements of the stems after welding from 0 to 14 cycles, data from Table 2

Fig. 7 Comparison of electrolytic a) nitric acid and b) oxalic acid etching on a three cycle weld. The nitric shows the grain size more clearly while the oxalic shows deformation twinning more clearly.

Fig. 8 X-ray images of the welds in the edge and plan view showing closure lengths after a) 1 cycle, b) 4 cycles c) 6 cycles and d) 12 cycles

Fig. 9 High magnification images in the crow's foot of stem samples as a function of cycles for nitric acid etchant after a) 0 cycles, b) 3 cycles, c) 4 cycles, d) 6 cycles, e) 8 cyles, f) 12 cycles, and g) 14 cycles.

Fig. 10 Images of the closure at the center of the pinch weld showing deformation bands microstructure evolution after a) 3 cycles, b) 4 cycles, c) 5 cycles and d) 7 cycles.

Fig. 11 Heat affected zone and grain size model based on the Avrami Equation

Fig. 12 The dynamic resistance decreases, and the net displacement increases with increasing cycles after the second cycle

Fig. 13 Typical displacement curve and current data for a 12 cycle weld showing the electrode movement during and after the weld

Table Caption List

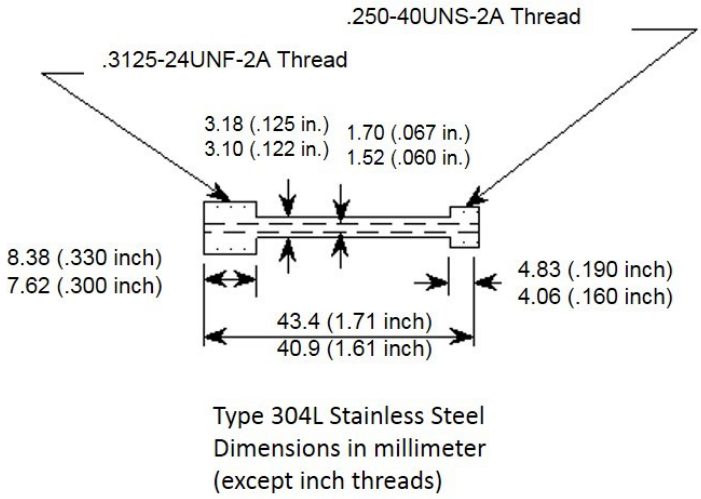

Fig. 1: Geometry of stems used in this study

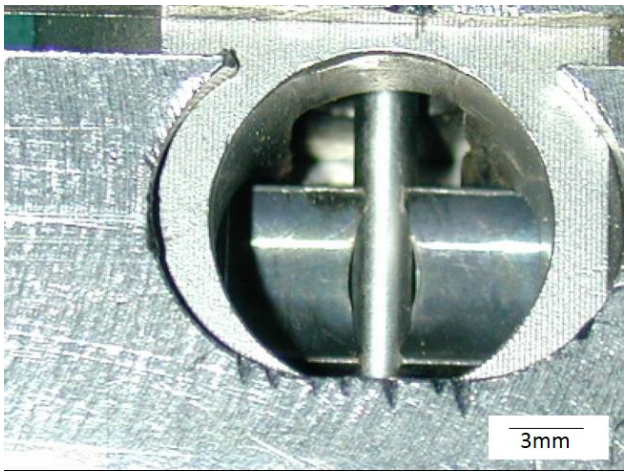

Fig. 2 Stem and confining dies used in this study to make confined pinch weld

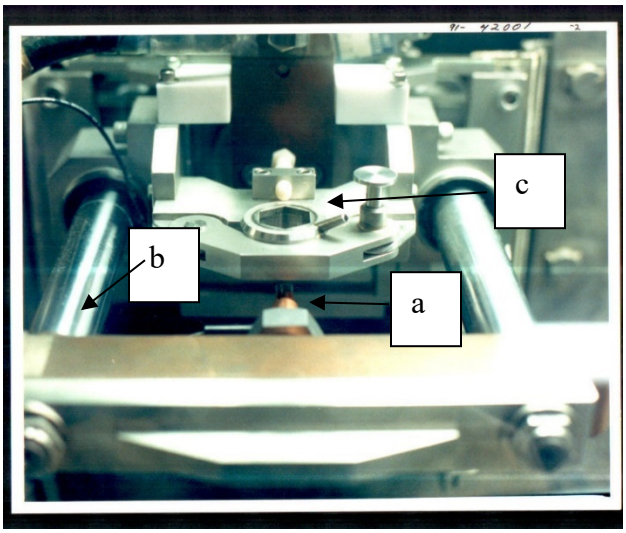

Fig. 3 Weld head used in this study, a indicates the PW electrode, b the ram that applies the force, and c the weld fixture support

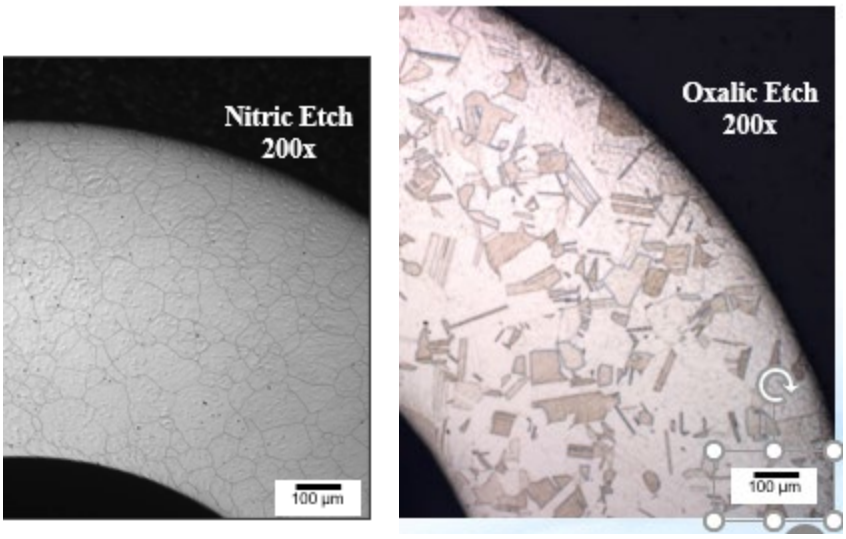

a b

Fig. 4. Initial microstructure of the stem electrolytically etched with a) nitric acid showing the grain size and b) etched with oxalic acid showing other microstructural details

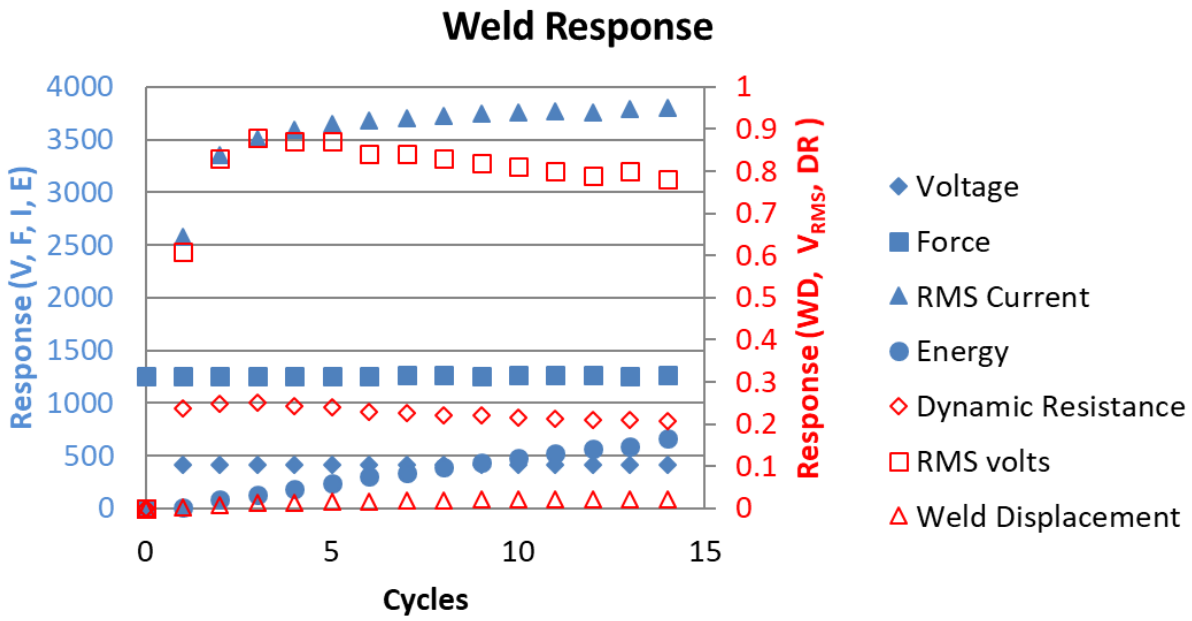

Fig. 5 Plot of weld conditions, data from Table 1

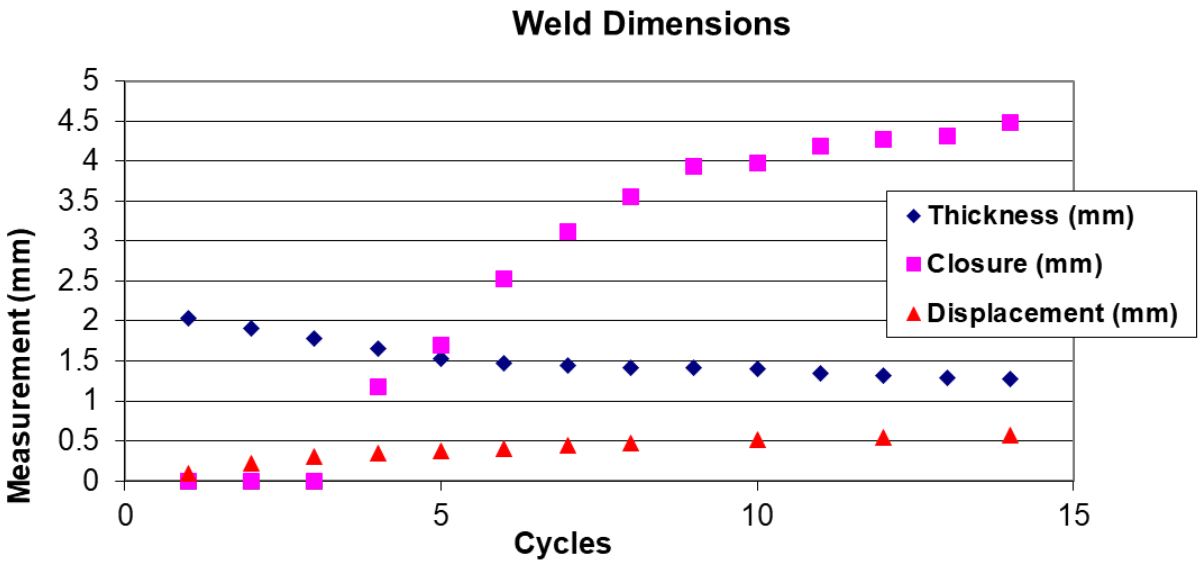

Fig. 6 Dimensional measurements of the stems after welding from 0 to 14 cycles, data from Table 2

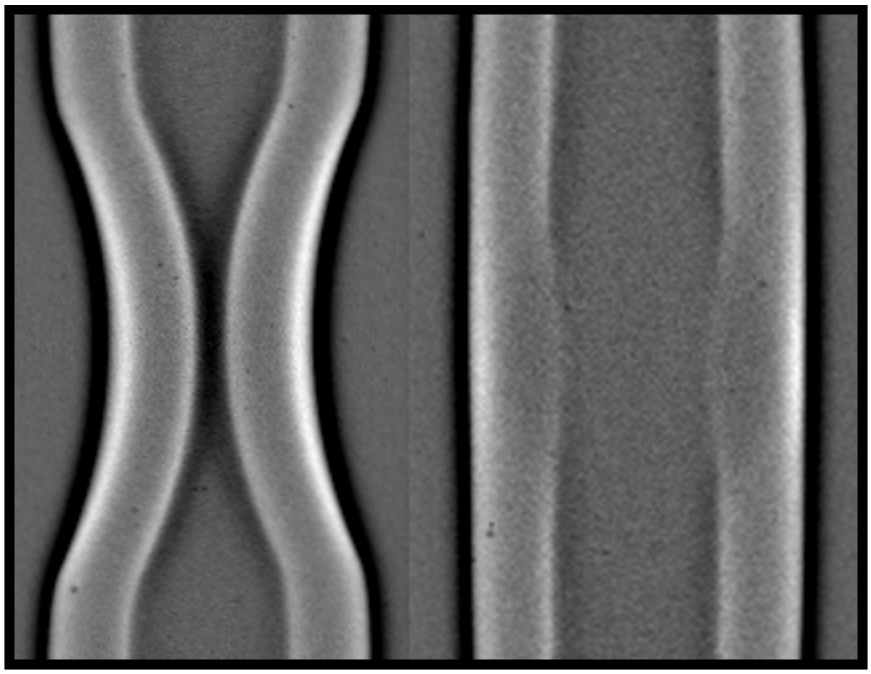

(a)

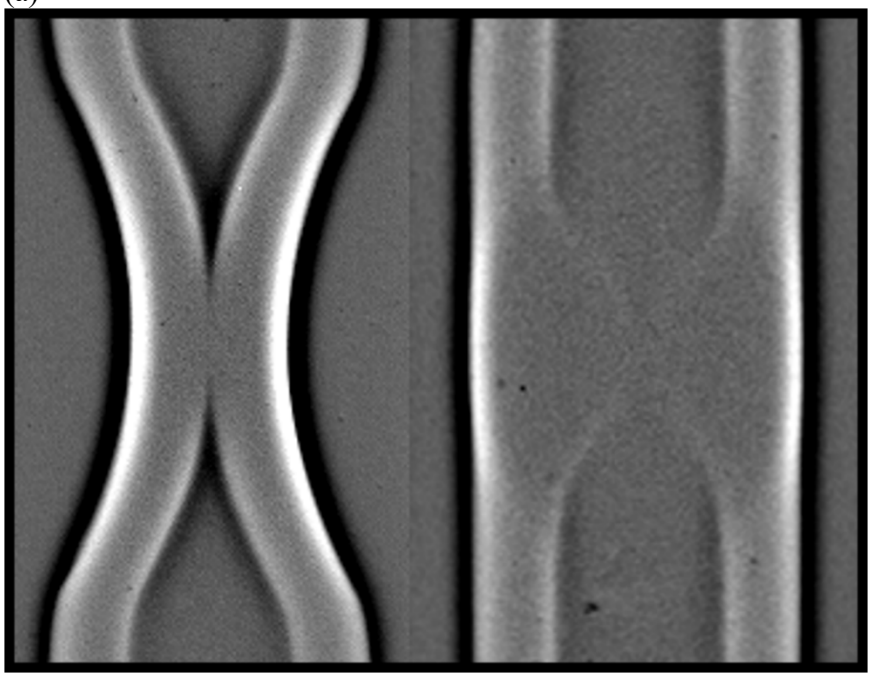

(b)

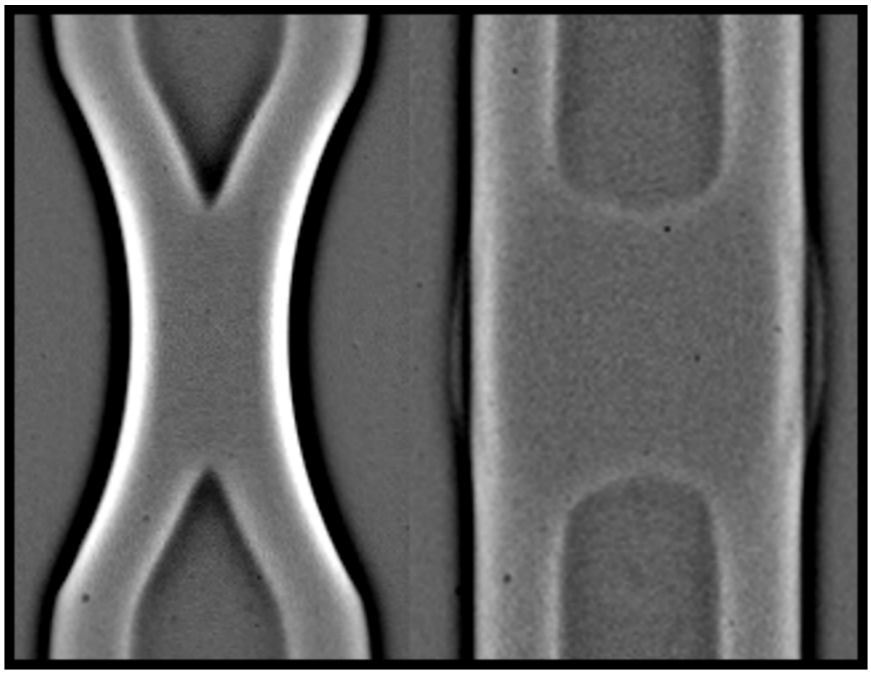

(c)

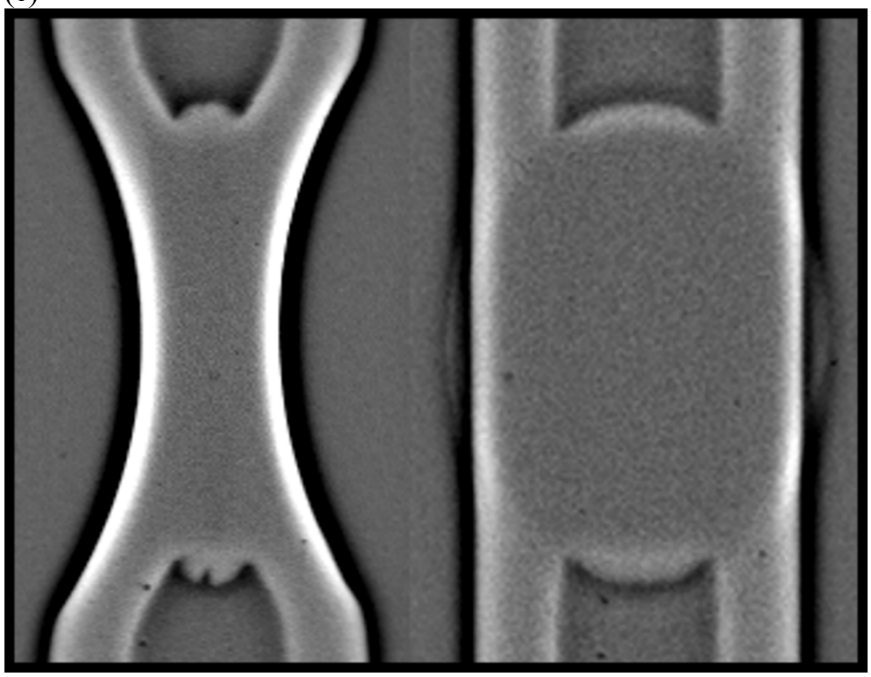

(d)

Fig. 7 X-ray images of the welds in the edge and plan view showing closure lengths after a) 1 cycle, b) 4 cycles c) 6 cycles and d) 12 cycles

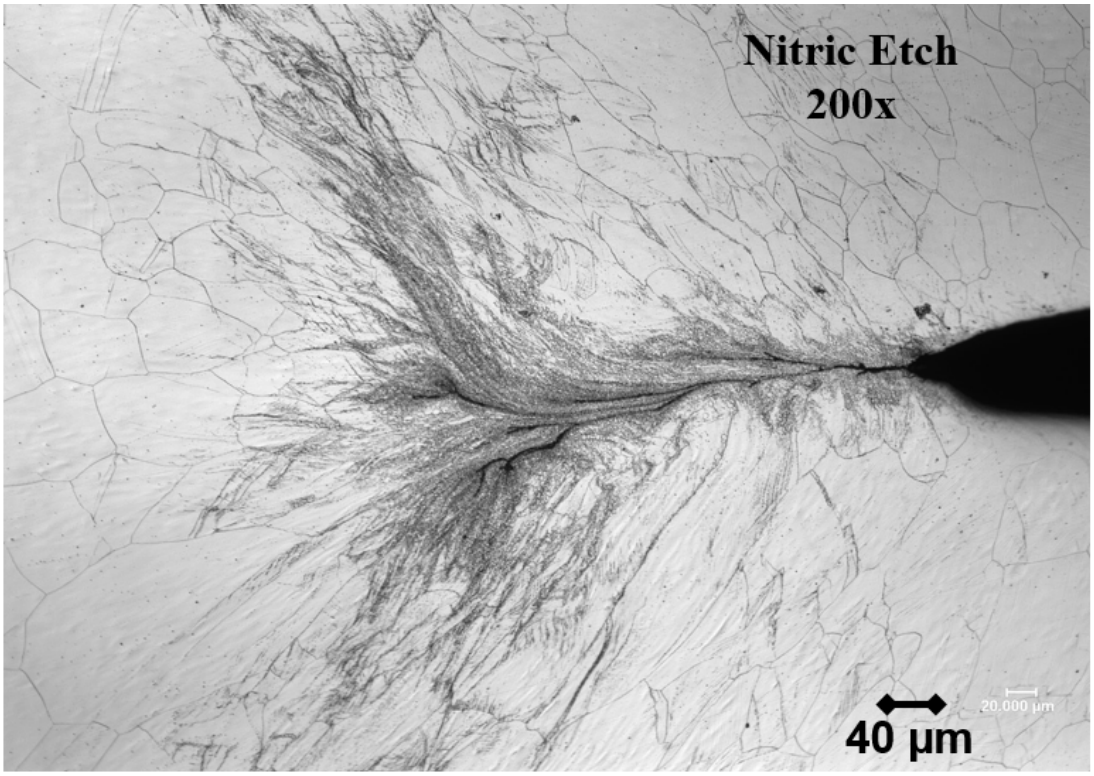

(a)

(b)

Figure 8. Comparison of electrolytic a) nitric acid and b) oxalic acid etching on a three cycle weld. The nitric shows the grain size more clearly while the oxalic shows deformation twinning more clearly.

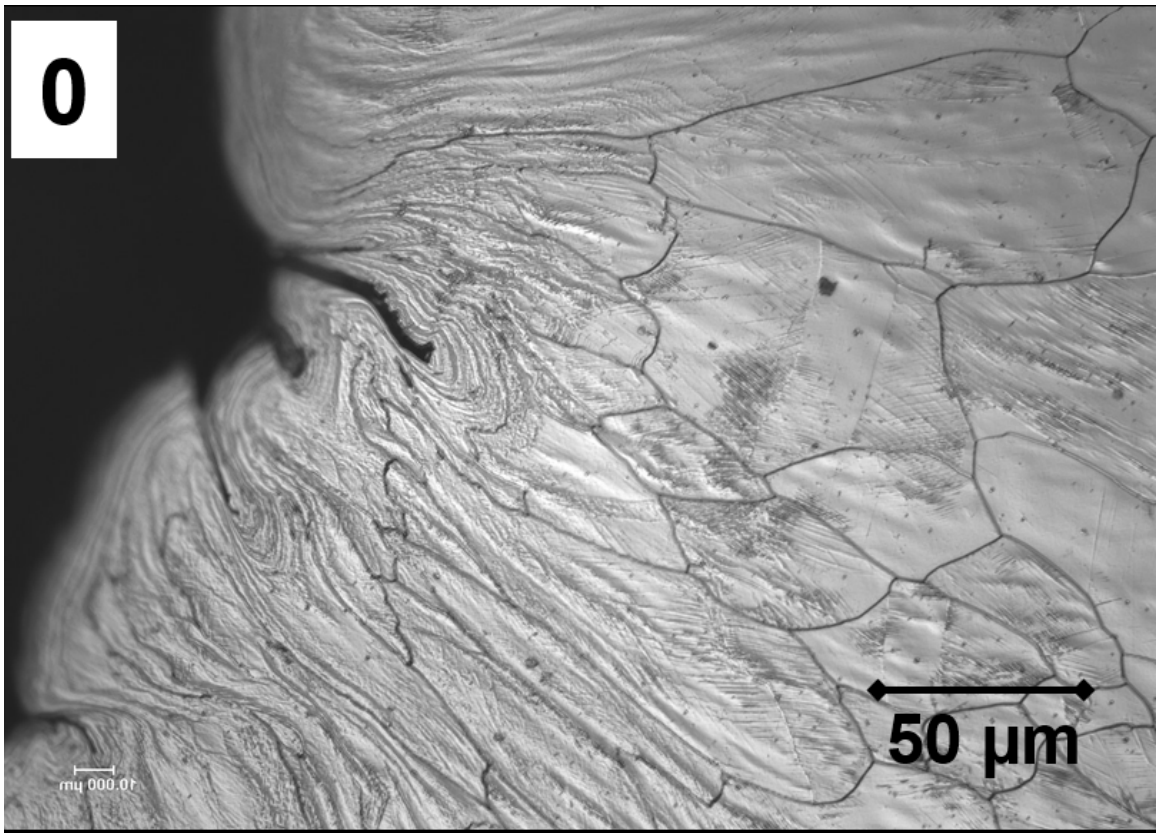

(a)

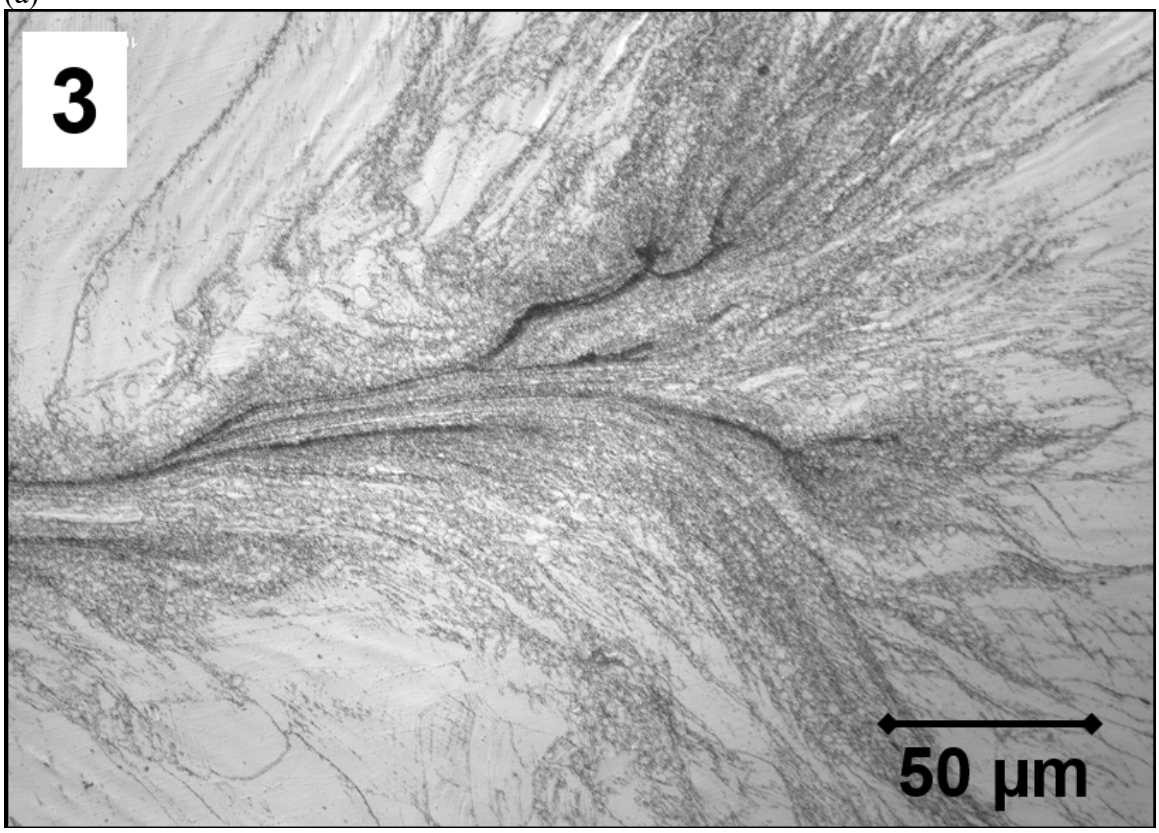

(b)

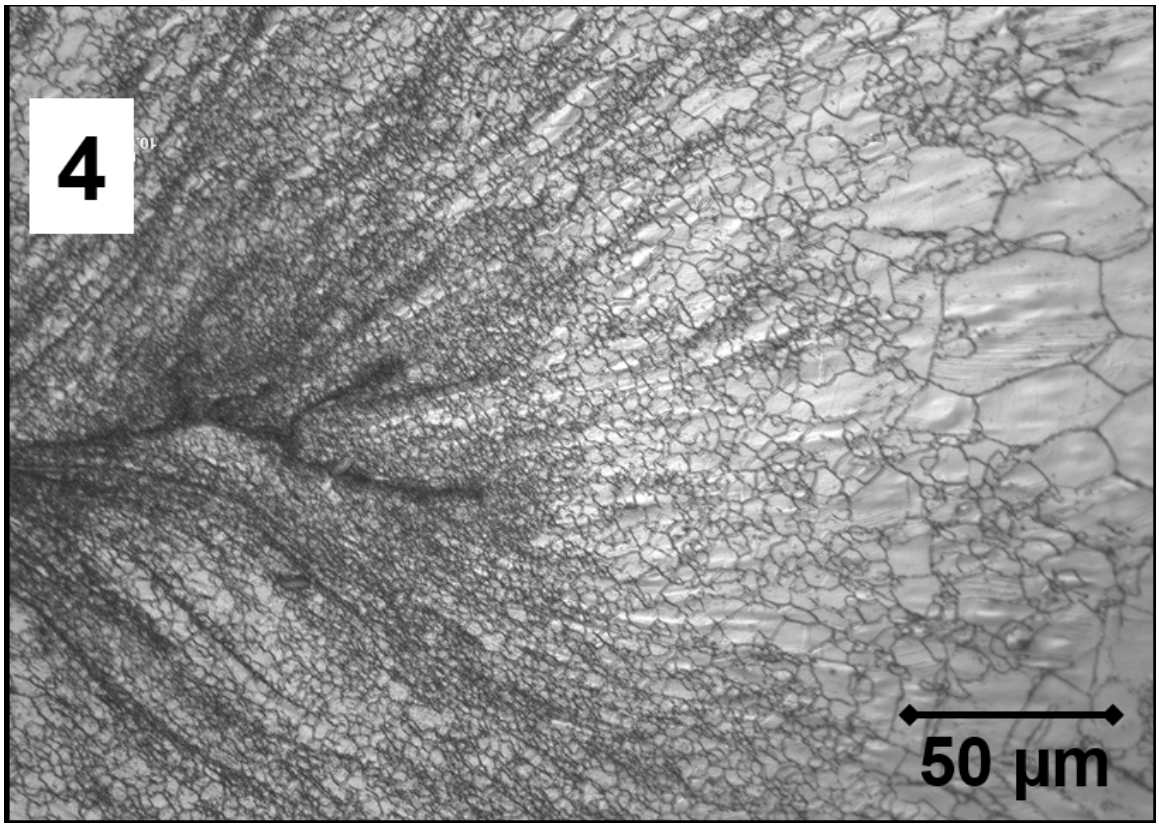

(c)

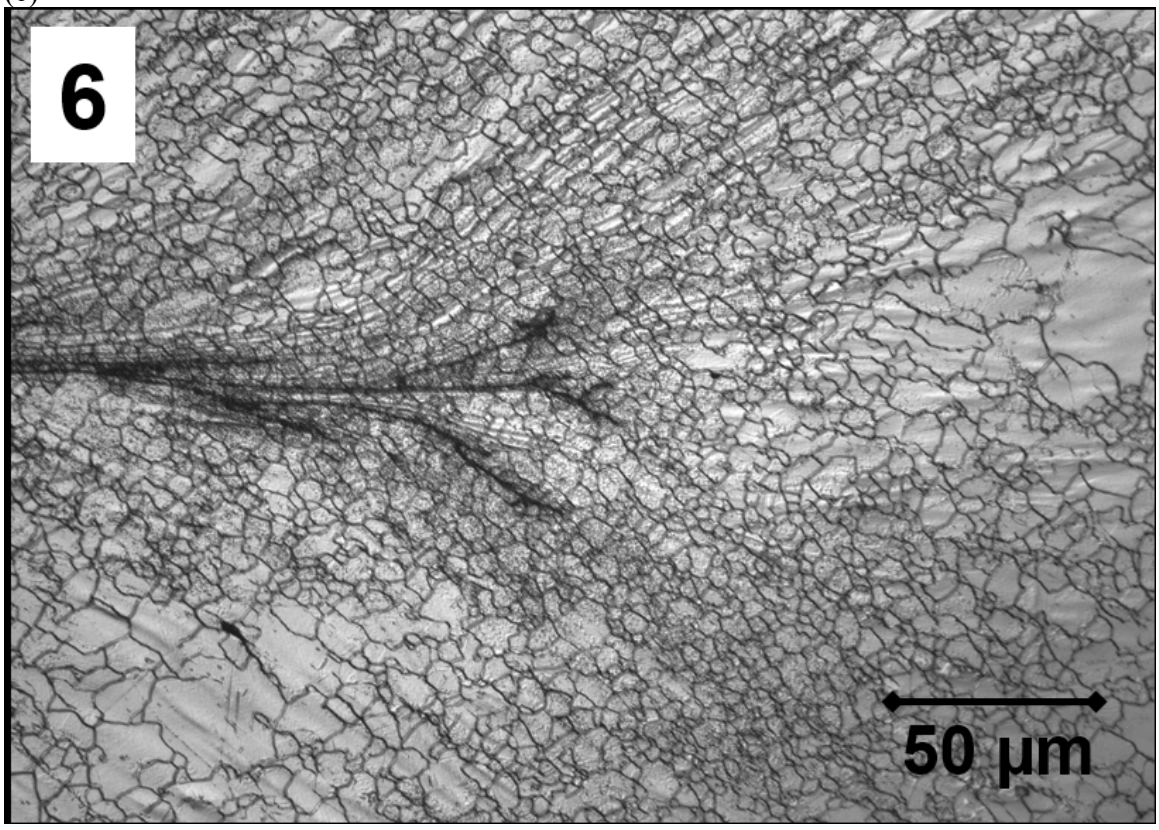

(d)

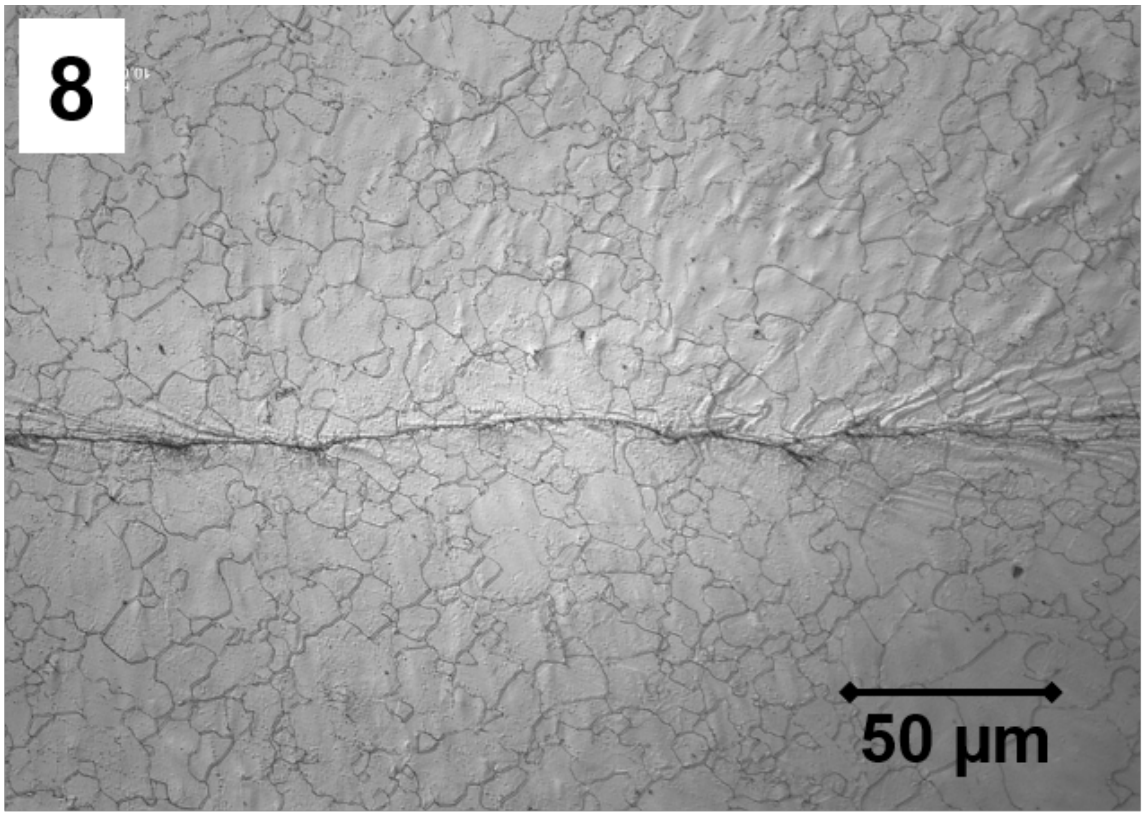

(e)

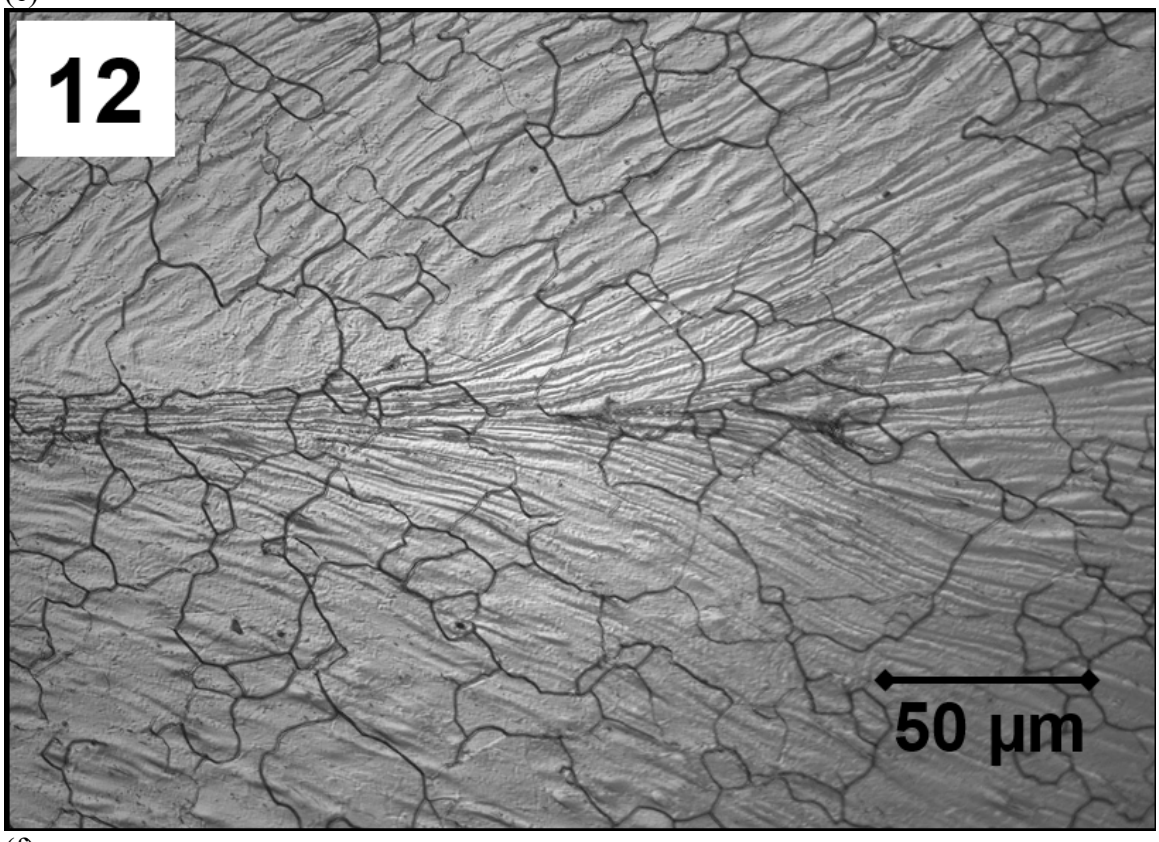

(f)

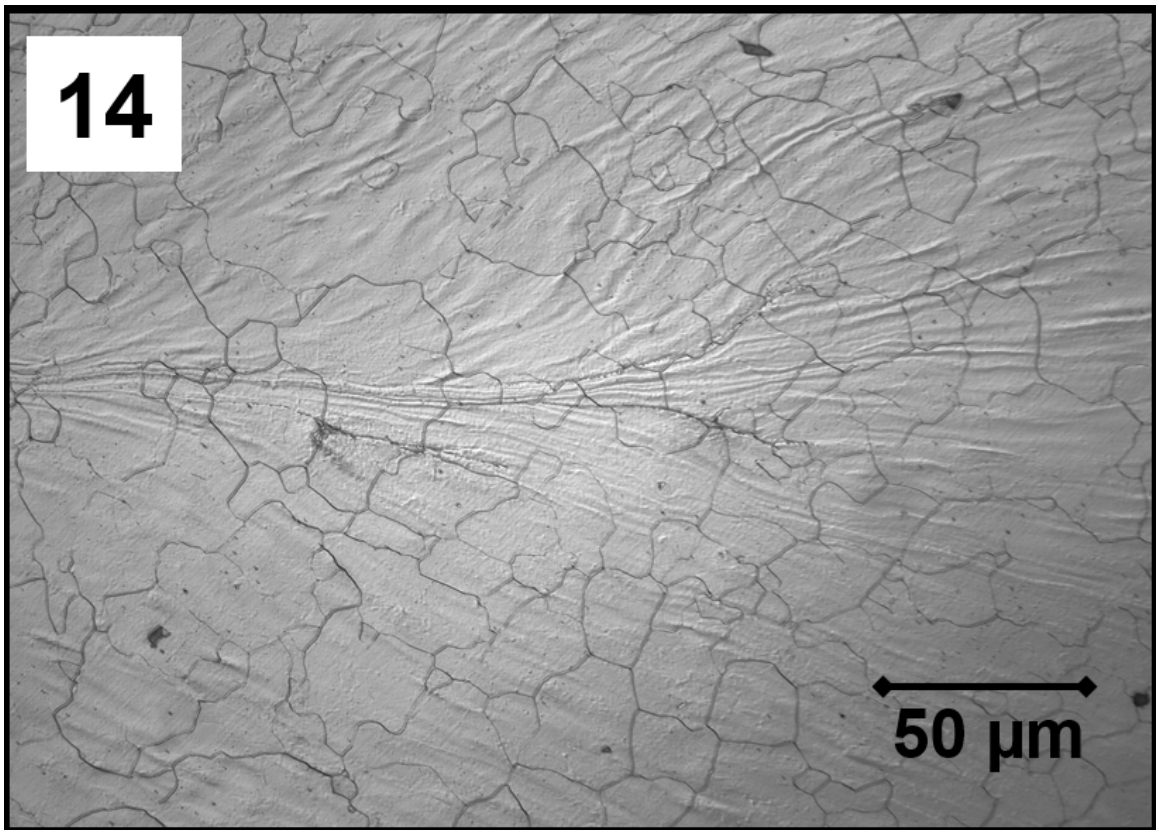

(g)

Fig. 9 High magnification images in the crow's foot of stem samples as a function of cycles for nitric acid etchant after a) 0 cycles, b) 3 cycles, c) 4 cycles d) 6 cycles, e) 8 cycles,)f) 12 cycles, and g) 14 cycles.

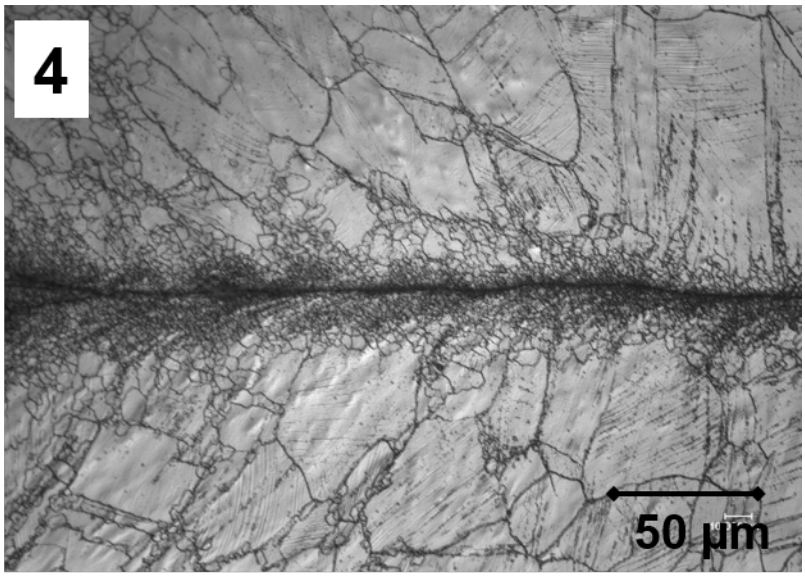

(a)

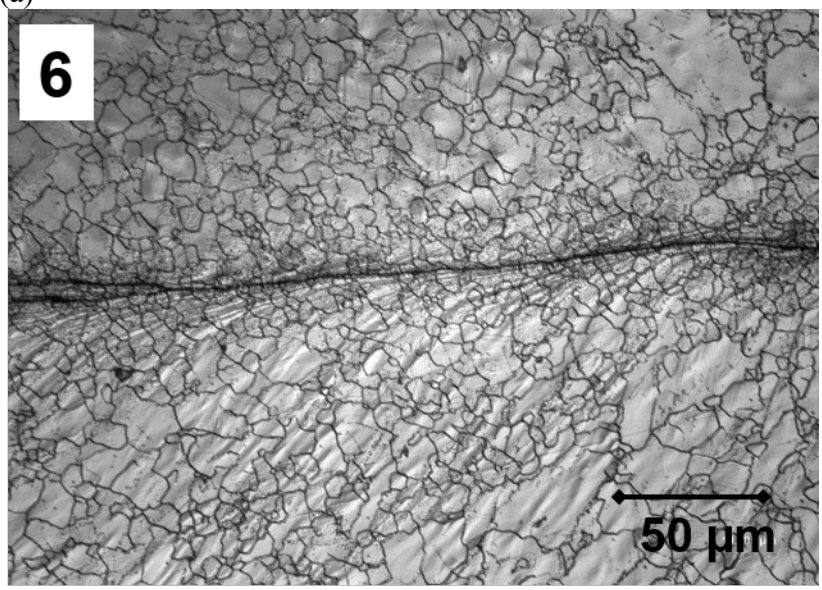

(b)

Fig. 10 Images of the closure at the center of the pinch weld exhibiting a different morphology than in the crow's foot after a) 4 cycles, b) 6 cycles

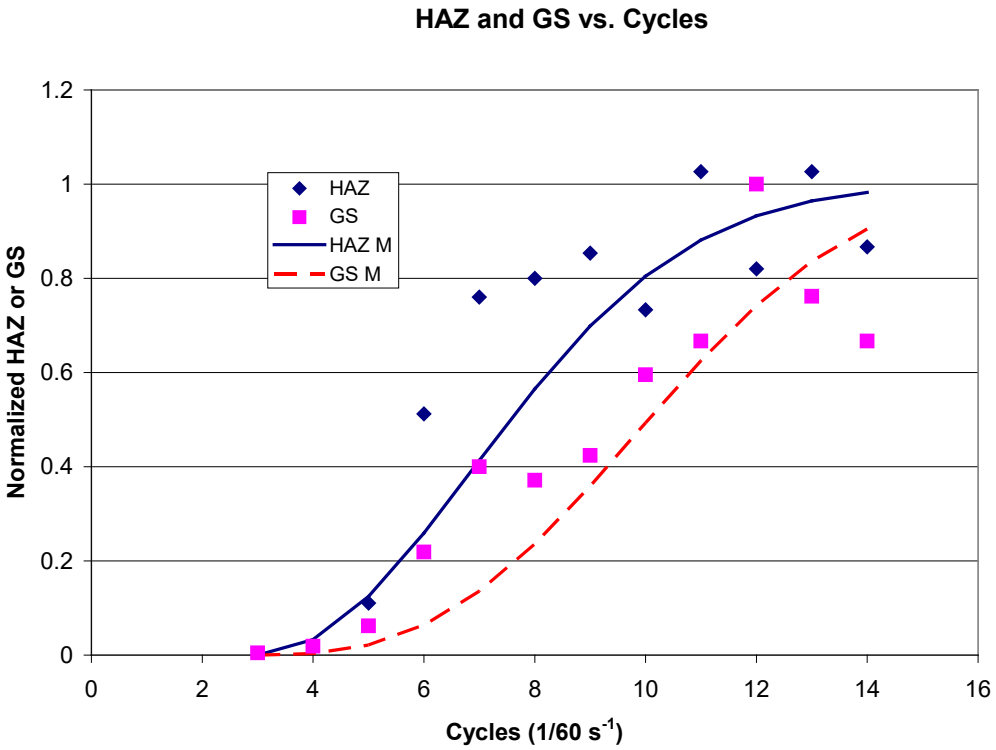

Fig. 11 Heat affected zone and grain size model based on the Avrami Equation

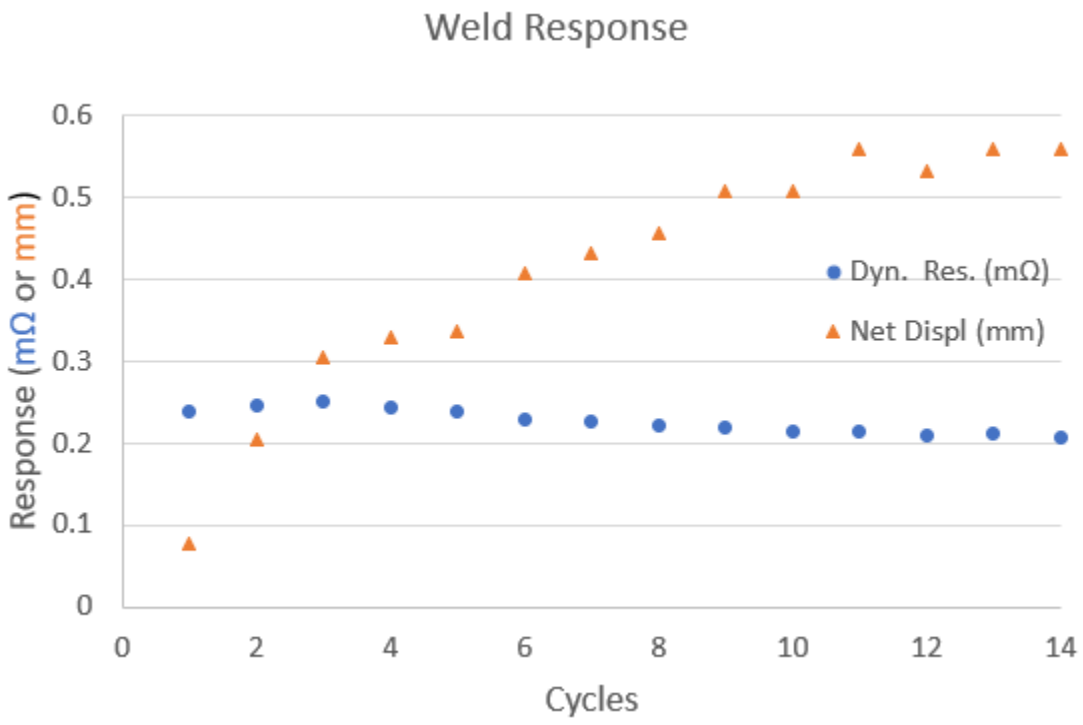

Fig. 12 The dynamic resistance decreases and the net displacement increases with increasing cycles after the second cycle

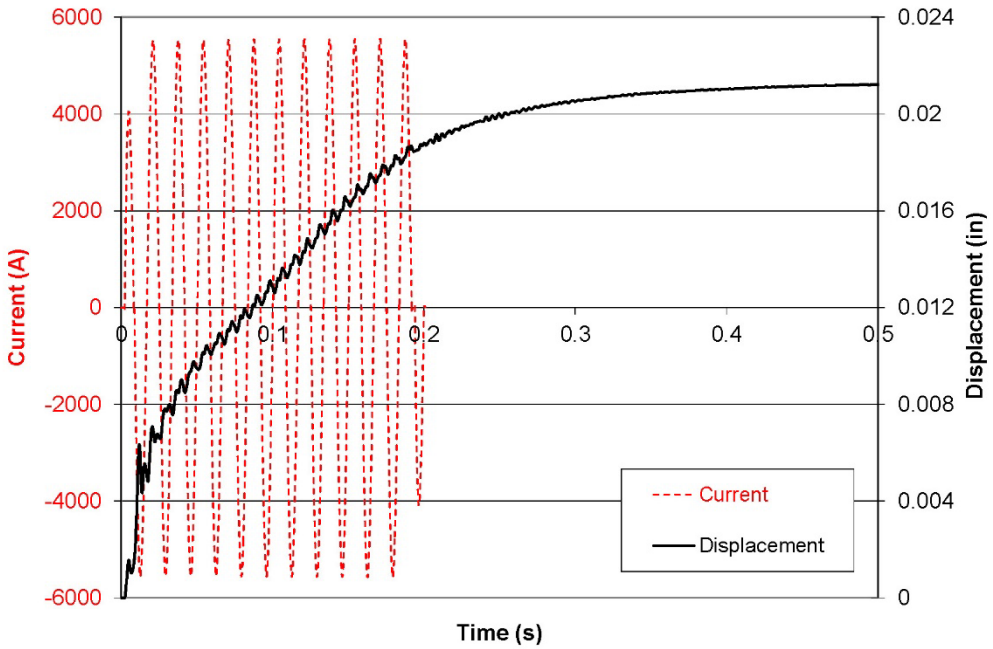

Fig. 13 Typical displacement curve and current data for a 12 cycle weld showing the electrode movement during and after the weld

Table 1. Weld conditions and results from the data acquisition system

Serial No.	Cycles	Voltage (V)	Force (N)	RMS Current (A)	Dyn. Res. (mΩ)	Energy (J)	RMS Volts	Net Displ (mm)
20641	1	415.2	5587	2574	0.238	12.7	0.612	0.076
20451	2	414.7	5593	3352	0.247	87.2	0.828	0.203
X0130	3	415.1	5590	3501	0.250	130.4	0.875	0.305
20539	4	414.9	5594	3589	0.243	184.8	0.871	0.330
20477	5	415.4	5577	3649	0.239	240.1	0.871	0.336
20502	6	415.4	5591	3684	0.229	301.0	0.844	0.406
X0100	7	414.6	5586	3705	0.227	339.5	0.841	0.432
X0107	8	414.8	5587	3722	0.222	386.3	0.827	0.457
20469	9	415.1	5579	3741	0.220	434.8	0.824	0.508
X0120	10	415.0	5582	3756	0.214	475.8	0.805	0.508
X0127	11	415.7	5584	3771	0.213	526.2	0.804	0.559
X0101	12	413.7	5590	3762	0.210	565.5	0.791	0.533
X0126	13	NA	NA	3794	0.211	583.2	0.801	0.559
X0117	14	413.8	5589	3804	0.206	663.0	0.784	0.559

Table 2: Dimensional measurements of stems after welding from 0 to 14 cycles.

N	Weld ID (stem)	Thick (mm)	C L. (mm)
0	X0106	NA	0.000
1	20461	2.032	0.000
2	20451	1.905	0.000
3	X0130	1.778	0.000
4	20539	1.651	1.168
5	20477	1.524	1.702
6	20502	1.473	2.540
7	X0100	1.448	3.124
8	X0107	1.422	3.556
9	20469	1.422	3.937
10	X0120	1.397	3.988
11	X0127	1.346	4.191
12	X0101	1.321	4.267
13	X0126	1.295	4.318
14	X0117	1.270	4.470

N is number of weld cycles @60 Hz, Thick is post weld thickness, and CL is closure length measured radiographically,

Typical Standard Deviations for the measurements, based on four welds made at 3415 A, 12 cycles, 339 V, are as follows (6):
Thickness: 53 μm
Closure Length: 21 μm

Table 3. Additional weld quality metrics for inspection

Serial Number	Cycles	Weld Thickness	Closure	Extrusion	E/B	.25 mm ball test
	(n)	mm	mm	mm	mm	mm
X0109	0	NA	0	0	0	0
X0106	0	NA	0	0	0	0
20461	1	2.032	0	0	0	0
20451	2	1.905	0	0	0	0
X0130	3	1.778	0	0	0	0
20539	4	1.651	1.1684	0	0	0.127
20477	5	1.524	1.7018	0	0	0.1016
20502	6	1.4732	2.54	0	0	0.127
X0100	7	1.4478	3.1242	0	0	0.2286
X0107	8	1.4224	3.556	0	0	0.4572
20469	9	1.4224	3.937	0.04572	2.794	NA
X0120	10	1.397	3.9878	0.08636	4.826	NA
X0127	11	1.3462	4.191	0.16256	7.366	NA
X0101	12	1.3208	4.2672	0.12446	5.588	NA
X0126	13	1.2954	4.318	0.18796	7.874	NA
X0117	14	1.27	4.4704	0.21336	8.128	NA